A Massive AGB Donor in Scutum X-1: Identification of the First Mira Variable in an X-Ray Binary

Kishalay De[1,10] ⬤, Deepto Chakrabarty[1] ⬤, Roberto Soria[2,3] ⬤, Michael C. B. Ashley[4] ⬤, Charlie Conroy[5] ⬤, Matthew J. Hankins[6] ⬤, Mansi M. Kasliwal[7] ⬤, Ryan M. Lau[8], Anna M. Moore[9], Robert Simcoe[1] ⬤, Jamie Soon[9], and Tony Travouillon[9] ⬤

[1] MIT-Kavli Institute for Astrophysics and Space Research, 77 Massachusetts Avenue, Cambridge, MA 02139, USA; kde1@mit.edu
[2] College of Astronomy and Space Sciences, University of the Chinese Academy of Sciences, Beijing 100049, People's Republic of China
[3] Sydney Institute for Astronomy, School of Physics A28, The University of Sydney, Sydney, NSW 2006, Australia
[4] School of Physics, University of New South Wales, Sydney NSW 2052, Australia
[5] Harvard-Smithsonian Center for Astrophysics, Cambridge, MA 02138, USA
[6] Arkansas Tech University, Russellville, AR 72801, USA
[7] Cahill Center for Astrophysics, California Institute of Technology, 1200 E. California Boulevard, Pasadena, CA 91125, USA
[8] Institute of Space & Astronautical Science, Japan Aerospace Exploration Agency, 3-1-1 Yoshinodai, Chuo-ku, Sagamihara, Kanagawa 252-5210, Japan
[9] Research School of Astronomy and Astrophysics, Australian National University, Canberra, ACT 2611, Australia

Abstract

The symbiotic X-ray binary Sct X-1 was suggested to be the first known neutron star accreting from a red supergiant companion. Although known for nearly 50 yr, detailed characterization of the donor remains lacking, particularly due to the extremely high reddening toward the source ($A_V \gtrsim 25$ mag). Here, we present (i) improved localization of the counterpart using Gaia and Chandra observations, (ii) the first broadband infrared spectrum ($\approx$1–5 μm; $R \approx 2000$) obtained with SpeX on the NASA Infrared Telescope Facility, and (iii) the J-band light curve from the Palomar Gattini-IR survey. The infrared spectrum is characterized by (i) deep water absorption features (H_2O index $\approx 40\%$), (ii) strong TiO, VO, and CO features, and (iii) weak/absent CN lines. We show that these features are inconsistent with known red supergiants but suggest an M8-9 III–type O-rich Mira donor star. We report the discovery of large-amplitude ($\Delta J \approx 3.5$ mag) periodic photometric variability, suggesting a pulsation period of 621 ± 36 (systematic) ± 8 (statistical) days, which we use to constrain the donor to be a relatively luminous Mira ($M_K = -8.6 \pm 0.3$ mag) at a distance of $3.6^{+0.8}_{-0.7}$ kpc. Comparing these characteristics to recent models, we find the donor to be consistent with a $\approx$3–5 $M_\odot$ star at an age of $\approx$0.1–0.3 Gyr. Together, we show that Sct X-1 was previously misclassified as an evolved high-mass X-ray binary; instead, it is an intermediate-mass system with the first confirmed Mira donor in an X-ray binary. We discuss the implications of Mira donors in symbiotic X-ray binaries and highlight the potential of wide-field infrared time-domain surveys and broadband infrared spectroscopy to unveil their demographics.

Unified Astronomy Thesaurus concepts: X-ray binary stars (1811); Mira variable stars (1066); Sky surveys (1464); Asymptotic giant branch (108)

Supporting material: data behind figures

1. Introduction

Scutum X-1 was identified from a sounding rocket experiment nearly 50 yr ago (Hill et al. 1974) as an unusual and bright X-ray source exhibiting the strongest absorption ever detected at the time. The source has been subsequently detected by several X-ray missions (see Kaplan et al. 2007 for a review) and has been noted for exhibiting a conspicuous $\approx$112 s X-ray pulsation arising from a neutron star (NS) accretor (Koyama et al. 1991). Kaplan et al. (2007) presented the first accurate (to $\approx 1''$) X-ray localization using XMM-Newton observations, which positioned the X-ray source to be within $0.''2$ of a bright infrared counterpart ($K_s \approx 6.5$ mag) in the 2MASS catalog. The counterpart was reported to be nearly invisible in the optical bands ($r > 25.2$ mag, $i \approx 23.6$ mag;

Kaplan et al. 2007). Based on the extremely red colors ($J - K \approx 5.5$ mag), HK-band spectroscopy, and observed X-ray absorption, they suggested the counterpart to likely be a late-type supergiant with a two-dimensional classification of $\approx$M0-1 Ia-Iab. The source was thus classified as a symbiotic X-ray binary (SyXRB; Masetti et al. 2006) at a distance of 4–10 kpc and behind an extinction column of $A_V \gtrsim 25$ mag.

The suggested classification makes Sct X-1 the first known candidate for an NS accreting from the wind of a red supergiant (RSG) in a Galactic X-ray binary[11] and an evolved member of the high-mass X-ray binary (HMXB) population. The source still remains one of only three such known systems—the other two sources being the Galactic center X-ray binary CXO 174528.79–290942.8 (Gottlieb et al. 2020) and 4U 1954+31 for which the donor classification was only recently revised from an M4-5 III giant (Masetti et al. 2006) to an M4 I supergiant (Hinkle et al. 2020). Unlike the more common B-supergiant HMXBs (Martínez-Núñez et al. 2017), RSG HMXBs are rare due to their short lifetimes but are of

---

[10] NASA Einstein Fellow.

[11] The SIMBAD database lists Sct X-1 as an HMXB.

interest as ubiquitous evolutionary phases in the path from massive binaries to double compact objects (Mondal et al. 2020).

As noted in Kaplan et al. (2007), the spectrum used to classify the donor in Sct X-1 has uncertain flux calibration as well as limited wavelength coverage. In addition, the high reddening toward the source precludes any attempts at optical spectroscopy or photometry to constrain the donor type via spectral features or variability. Concomitantly, the Gaia catalog does not provide a parallax to constrain its distance and luminosity. The emergence of long-term infrared time-domain surveys combined with moderate-aperture infrared spectroscopy offers new opportunities to revisit the demographics of obscured Galactic X-ray sources such as Sct X-1.

In this paper, we present the first broadband infrared spectrum and near-infrared (NIR) light curve of the infrared counterpart of Sct X-1. Using the observed strong molecular absorption features and large-amplitude photometric variability, we show that Sct X-1 has been long misclassified as an RSG X-ray binary and instead contains a very late-type pulsating Mira donor star. We present the observational data in Section 2. Section 3 presents an analysis of the infrared spectral features and photometric variability to constrain the donor type, distance, and extinction. We discuss the implications of these results and summarize our findings in Section 4.
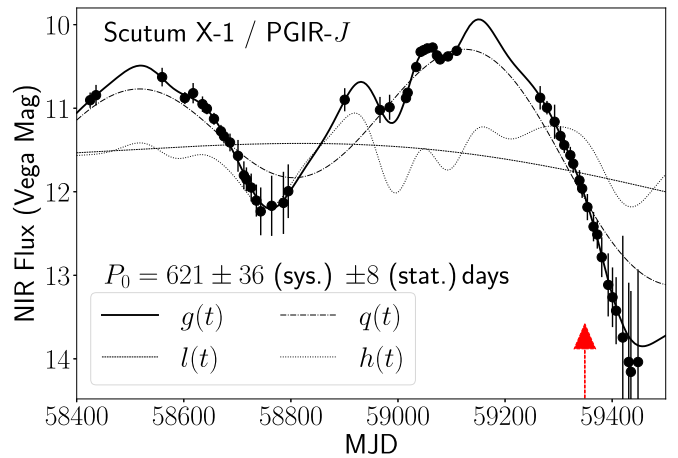
2. Observations

2.1. Infrared Photometry

Kaplan et al. (2007) showed that the source 2MASS J18352582–0736501 (hereafter 2MASSJ1835) was very likely (chance probability $\sim 2 \times 10^{-6}$) the infrared counterpart of Sct X-1, with a 2MASS magnitude of $J \approx 12$ mag. The sky location was monitored as part of regular survey operations of the Palomar Gattini-IR NIR time-domain survey (Moore & Kasliwal 2019; De et al. 2020). Palomar Gattini-IR is a wide-field (≈ 25 deg^2) and shallow J-band survey (reaching $J \approx 13$ mag and $J \approx 15$ mag[12] in and outside the Galactic plane, respectively), monitoring the entire visible sky from Palomar Observatory using a 30 cm telescope with a cadence of ≈ 2 nights. The light curve was obtained by performing forced aperture photometry at the location of the infrared counterpart, with an aperture size of $8.''3$. The light curve is shown in Figure 1 and was binned over ≈ 7 days intervals to improve the signal-to-noise ratio.

2.2. Infrared Spectroscopy

We obtained an infrared spectrum of 2MASSJ1835 using SpeX on the NASA Infrared Telescope Facility (Rayner et al. 2003; Program 2021A083, PI: De) on UT 2021 May 16. The data were obtained with a $0.''3$ slit, in both the SXD and LXD_long modes over multiple dithered exposures amounting to a total exposure time of ≈ 720 s and ≈ 300 s, respectively. The standard stars HIP 90967 and HIP 87108 were used for telluric and flux calibration in the SXD and LXD_long modes, respectively. The combined spectrum covers the full wavelength range of the instrument from ≈ 0.8 to ≈ 5.0 μm with a resolution of $R \approx 2000$. The data were reduced using the spextool pipeline (Cushing et al. 2004), while telluric and

---

[12] Vega magnitudes calibrated to the 2MASS photometric system are used throughout this paper.

Figure 1. PGIR J-band light curve of 2MASSJ1835. The black points denote the observed J-band photometry. The black solid line shows the best-fit semiparametric Gaussian process regression model ($g(t)$; see text). The black dashed, dotted–dashed and dotted lines denote the contribution from the long-term trend component ($l(t)$), primary periodic component ($q(t)$), and high-frequency variability component ($h(t)$), respectively. The best-fit period and its uncertainty are shown. The red arrow shows the SpeX observation epoch.

(The data used to create this figure are available.)

flux calibration was performed using the xtellcor package (Vacca et al. 2003). Due to the high reddening, the source is not detected at <1.0 μm in the final spectrum shown in Figures 2 and 3 (observation epoch is shown with a red arrow in Figure 1). The average signal-to-noise ratio is ≈ 300 in the K band, ≈ 200 in the H band, and ≈ 70 in the J band.

2.3. X-Ray Observations

The Chandra X-ray Observatory observed Sct X-1 on 2020 November 9 (ObsID 22417). The exposure started at MJD 59162.08 for a live time of 27.3 ks. The live time was 27.3 ks. The source was located at the aim point on chip S3 of the Advanced CCD Imaging Spectrometer array. We downloaded the data from the public archive and processed them with the Chandra Interactive Analysis of Observations (CIAO) software version 4.12 (Fruscione et al. 2006), with calibration database version 4.9.1. We rebuilt a level 2 event file with the task chandra_repro and created images in different energy bands with dmcopy. We built background-subtracted spectra and associated response and ancillary response files with specextract. We regrouped the spectrum to at least one count per bin, with the FTOOLS task grppha and fitted it with XSPEC (Arnaud 1996) version 12.11.0 using the Cash statistics (Cash 1979).

3. Analysis

3.1. Improved Localization and Recent X-Ray Flux

2MASSJ1835 is detected as a faint source in Gaia EDR3 (Gaia Collaboration et al. 2021) at the J2000 position $\alpha = 18{:}35{:}25.82$, $\delta = -07{:}36{:}50.4$ at a Gaia magnitude of $G \approx 20.5$. We used the CIAO analysis tools within the DS9 imaging package to determine the centroid of the point-like X-ray source in the 0.3–7 keV band Chandra data. The X-ray source centroid is measured to be $\alpha = 18{:}35{:}25.82$, $\delta = -07{:}36{:}50.6$. We cannot improve on the default Chandra astrometry because there are no other X-ray sources in the field
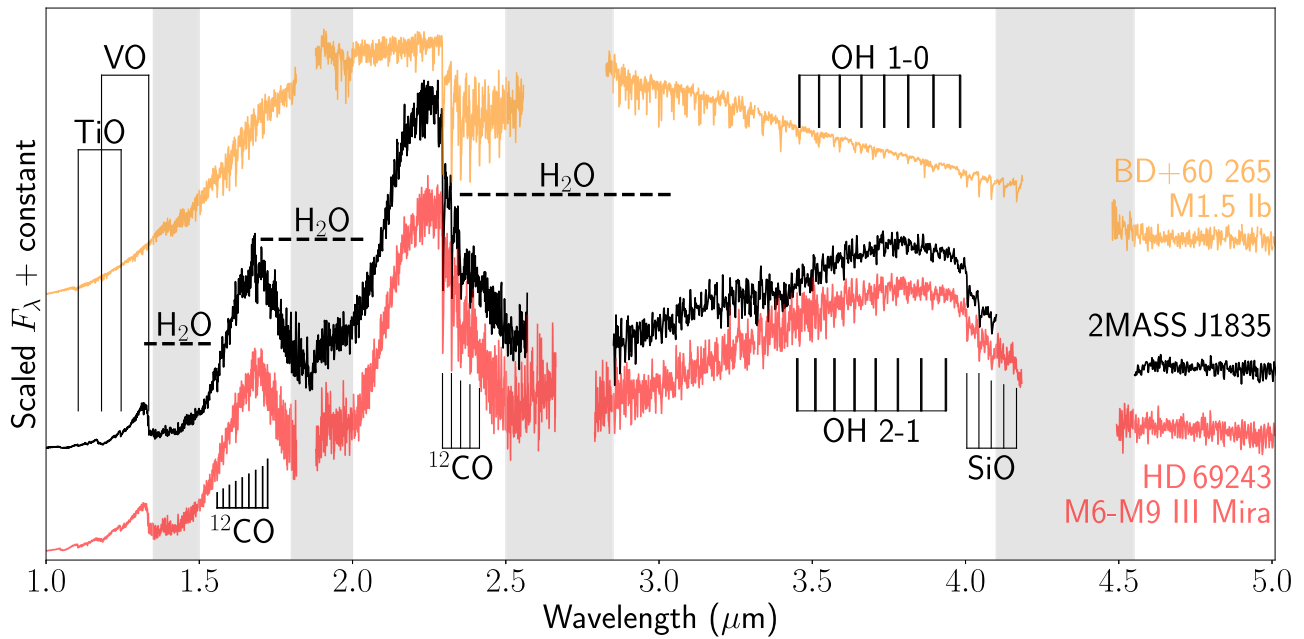
Figure 2. Comparison of the infrared spectrum of 2MASSJ1835 to that of an RSG (of the favored spectral type in Kaplan et al. 2007) and a late-type Mira variable (inferred from our analysis) in the IRTF Spectral Library (Rayner et al. 2009). Prominent absorption features are marked, while regions of low atmospheric transmission are shown in gray. The comparison spectra have been artificially reddened with $E(B - V) = 7.0$ mag based on the estimate in Kaplan et al. (2007) (see also Section 3.3).

(The data used to create this figure are available.)
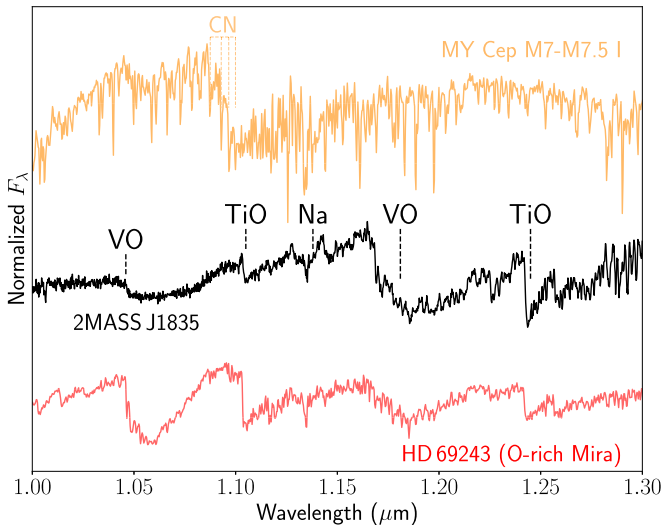
Figure 3. Comparison of the J-band spectrum of 2MASSJ1835 to that of a similar late-type supergiant (MY Cep) and Mira variable (HD 69243) in the IRTF spectral library. The spectra have been normalized by fitting the steep continuum with a low-order polynomial.

of view. Therefore, the position contains a default 90% uncertainty radius of $0''8$, improving on the $\approx 1''5$ (rms; Kirsch et al. 2004) positional uncertainty of previous XMM-Newton observations. The position is coincident within $\approx 0''2$ of the Gaia source and confirms the association proposed by Kaplan et al. (2007) with the excellent Chandra and Gaia astrometry.

Given the small number of counts (≈ 170 net counts), we used only two simple models for spectral fitting to estimate the recent X-ray flux. We tried power-law and bremsstrahlung models given the current low X-ray luminosity of the source. In both cases, we included a free photoelectric absorption

component, modeled with `tbabs`, with the abundances of Wilms et al. (2000). A power-law model with photon index $\Gamma = 1.9^{+0.9}_{-0.8}$ (90% confidence limit) and a bremsstrahlung model with $kT > 3.5$ keV, provide equally good fits (C statistics of 126.2/118 d.o.f, and 126.0/118 d.o.f., respectively). The column density of the neutral absorber is $N_{\rm H} = 5.6^{+2.4}_{-1.9} \times 10^{22}$ cm^{-2} for the power-law model and $N_{\rm H} = 5.2^{+1.8}_{-1.5} \times 10^{22}$ cm^{-2} for the bremsstrahlung model. The absorbed 0.3–10 keV flux is $\approx 2.0 \times 10^{-13}$ erg cm^{-1} s^{-1} in both cases. For the power-law model, this corresponds to a 0.3–10 keV unabsorbed flux of $6.3^{+15.0}_{-2.6} \times 10^{-13}$ erg cm^{-2} s^{-1} and for the bremsstrahlung model, of $4.6^{+2.1}_{-1.0} \times 10^{-13}$ erg cm^{-2} s^{-1}. The X-ray source has thus faded in flux by a factor of ~ 20–30 since the 2004 XMM-Newton observations (Kaplan et al. 2007), $\sim 100 \times$ compared with the 1987 GINGA observations (Koyama et al. 1991), and a few $\sim 1000 \times$ since its discovery in the 1970s (Hill et al. 1974).

3.2. Infrared Spectrum

The broadband infrared spectrum of 2MASSJ1835 is shown in Figure 2. The source exhibits a steep rising continuum from ≈ 1.0 to $\approx 2.3\ \mu$m, consistent with the high reddening reported by Kaplan et al. (2007). Superimposed on the rising continuum, the spectrum exhibits broad and deep absorption features around ≈ 1.4, $\approx 1.9\ \mu$m, and $\approx 2.7\ \mu$m, consistent with water absorption features seen in very late-type giants (Kleinmann & Hall 1986; Rayner et al. 2009). At shorter wavelengths, the strongest absorption features are the bandheads of TiO and VO (in the J band), while we identify absorption features of the second ^{12}CO overtone in the H band. The K band is dominated by conspicuous sharp features of the ^{12}CO first overtone series, while we detect features of the OH 1–0, 2–1, and SiO bandheads in the L band.

Although Kaplan et al. (2007) did not conclusively identify the spectral and luminosity class of 2MASSJ1835, they argued for similarity with those of early M-type supergiants based on the detection of metal features and strong ^{12}CO K-band features (Ramirez et al. 1997; Comerón et al. 2004). The ^{12}CO line equivalent width (EW) is known to increase with decreasing temperature and specific gravity, making it particularly well suited to identifying cool supergiants (Rayner et al. 2009). However, very late-type asymptotic giant branch (AGB) stars, typically appearing as Mira variables, also exhibit similarly strong (and variable) ^{12}CO features as supergiants (Blum et al. 2003; Comerón et al. 2004), making the previous classification unreliable.

Messineo et al. (2021) recently devised a classification method for giants, Miras, and supergiants using a large sample of IRTF spectra, particularly focusing on Mg I 1.71 μm to break the degeneracy between temperature and gravity. Based on this scheme, we measure a ^{12}CO EW of 50.5 ± 1.5 Å and a Mg I 1.71 μm EW of 3.0 ± 0.6 Å. The values place the source squarely in the phase space occupied by only supergiant stars and Mira AGB stars (see their Figure 17), ruling out the case for a normal giant. Strong water absorption features[13] are known to be seen only in large-amplitude pulsating variables ($\delta V > 1.7$ mag; Lançon & Wood 2000), which are formed in the propagating shocks in their dense extended atmospheres (Bessell et al. 1989). Based on the H_2O absorption index defined in Blum et al. (2003), we measure an absorption of $\approx 40\%$. The H_2O absorption index increases with decreasing effective temperature and decreasing luminosity (Lancon & Rocca-Volmerange 1992; Comerón et al. 2004); hence, the large absorption clearly suggests this source to be a very late-type Mira variable because supergiants exhibit absorption indices of $\lesssim 6\%$ (Messineo et al. 2021). Figure 2 shows a comparison of 2MASSJ1835 to that of the favored stellar type in Kaplan et al. (2007) and a late-type Mira variable, clearly demonstrating consistency with the latter.

Messineo et al. (2021) highlight additional differences between the NIR spectra of Miras and supergiants based on molecular features of VO, TiO, and CN in the J band. Figure 3 shows the J-band spectrum of 2MASSJ1835, highlighting deep absorption bandheads of VO and TiO, compared to that of a late-type supergiant and a Mira variable. The TiO bandheads near 1.25 μm are detected at spectral types M7 or later (Wright et al. 2010), while the VO features are known to become prominent at very low effective temperatures of $T_{\rm eff} \lesssim 3200$ K (spectral type M6 or later; Joyce et al. 1998). In particular, the TiO bandhead at ≈ 1.1 μm is only observed in the spectra of O-rich Mira AGBs, while the VO feature at ≈ 1.05 μm is strong in O-rich Mira AGBs but weak in supergiants (Messineo et al. 2021). RSGs also ubiquitously show CN absorption bandheads near ≈ 1.09 μm since their atmospheres are rich in CN molecules, which are clearly seen in the spectrum of the RSG but are weak/absent in 2MASSJ1835. We measure the EW of the CN absorption features using the J8 + J9 + J10 index defined in Messineo et al. (2021) and measure a value of 0.03 ± 1.07 Å, consistent with the phase space only occupied by Mira AGBs (see Figure 5 in Messineo et al. 2021). Overall, we conclude that the molecular absorption features in 2MASSJ1835 suggest a revised classification of the donor star to be an M8-9 III–type oxygen-rich Mira variable.

---

[13] Kaplan et al. (2007) also noted possible water absorption in their K-band spectra but were inconclusive due to uncertain flux calibration.

3.3. Infrared Light Curve

3.3.1. Periodicity Analysis

The well-sampled J-band light curve of 2MASSJ1835 is shown in Figure 1. The light curve shows a clear periodic trend superimposed by smaller-amplitude high-frequency oscillations. Noting the strong evidence for water absorption in the counterpart spectrum (see Section 3.2), we interpret the variability as large-amplitude pulsations of a Mira variable (Kholopov et al. 1985). Mira variables are known to be not strictly periodic but characterized by both low-frequency and high-frequency variations associated with variations in circumstellar dust and supergranular convection (Groenewegen et al. 2007; Iwanek et al. 2021). We use the semiparametric Gaussian process regression model proposed by He et al. (2016) to account for these variations, decomposing the light curve into four parts:

$$g(t) = m + l(t) + q(t) + h(t), \tag{1}$$

where m is the mean magnitude, $l(t)$ is the slowly variable mean magnitude, $q(t)$ is the primary periodic term, and $h(t)$ is the high-frequency stochastic variability. The terms are modeled Gaussian processes with different kernels to account for effects such as changing amplitudes across cycles.

We use the R code distributed by He et al. (2016) to derive a primary pulsation period from the log-likelihood periodogram and a best-fit J-band light-curve model including all the variability terms. We estimate the statistical uncertainty in the period by simulating 100 realizations of the observed light curve by adding Gaussian noise scaled to the photometric uncertainties. In order to estimate the systematic uncertainty given the relatively short baseline (≈ 1000 days) of our light curve, we selected two Mira variables (OGLE-BLG-LPV-180685 and GLE-LMC-LPV-00055) with similar light curves to Sct X-1 from the OGLE-III database (Udalski et al. 2008), scaled their well-known periods to 621 days, and then examined the scatter of periods found from about fifty 1000 day chunks uniformly distributed along the full light curves. The standard deviation of the periods was 28 days for OGLE-BLG-LPV-180685 and 36 days for OGLE-LMC-LPV-00055, and we thus take the larger as an estimate of the uncertainty. The best-fit light curve and period are shown in Figure 1. The observed peak-to-peak amplitude of $\Delta J \approx 3.5$ mag is consistent with the large-amplitude NIR variability seen in long-period symbiotic Miras (Gromadzki et al. 2009). We discuss the implications of the observed pulsation amplitude on the reported archival fluxes of 2MASS J1835 in the Appendix.

3.3.2. Distance and Extinction

Mira variables exhibit a period–luminosity–color relation over several decades in luminosity (Feast et al. 1989; Wood 2000), and that is commonly used to estimate distances to symbiotic Miras (Whitelock 1987; Gromadzki et al. 2009). Using the Whitelock et al. (2008) period–luminosity relation for O-rich Miras suggests an intrinsic absolute magnitude of $M_K = -8.6 \pm 0.3$ mag ($M_{\rm bol} \approx -5.1$). Our inferred NIR luminosity is marginally fainter than the supergiant luminosity ($M_K \approx -9.4$) class assumed in Kaplan et al. (2007). Using the period–color relation from Whitelock et al. (2000), we estimate an intrinsic NIR color of $(J - K)_0 = 1.59 \pm 0.26$ mag. The 2MASS J magnitude of the source is consistent with the long-term average observed in the PGIR light curve, and

hence we use the 2MASS measurements to infer a $E(J - K) = 3.92 \pm 0.27$ mag.

The estimated color excess corresponds to an optical extinction of $A_V = 21.8 \pm 1.5$ mag ($A_K = 2.4 \pm 0.2$ mag) using the same extinction law as in Kaplan et al. (2007). The estimate corroborates the previous suggestion that Sct X-1 lies behind a large column of dust. The observed K-band magnitude and inferred extinction place the source at a distance of $3.6^{+0.8}_{-0.7}$ kpc. The estimated distance is consistent with that estimated by Kaplan et al. (2007), due to the inferred K-band luminosity difference being compensated by the redder intrinsic color of the Mira. Applying the inferred extinction (we assume a Cardelli et al. 1989 extinction law with $R_V = 3.1$) to the observed 2MASS photometry and fitting a Planck function, we derive an NIR color temperature of $\approx 2000 \pm 190$ K, consistent with the effective temperatures of very late-type Mira variables (Haniff et al. 1995; Feast 1996). Overall, the long pulsation period and large amplitude are consistent with a very late-type Mira variable as inferred from the spectral analysis (Feast et al. 1989; Wood & Sebo 1996).

4. Discussion and Summary

We have presented spectroscopic and photometric evidence to suggest that the donor star in Sct X-1 is an M8-9 III–type pulsating Mira, revising the classification of Kaplan et al. (2007), who favored an RSG donor. Most SyXRB donors have been previously classified with early M-type red giant donors, similar to the first classified source GX 1+4 (Davidsen et al. 1977; Chakrabarty & Roche 1997) that was suggested to be at the tip of the first-ascent red giant branch. Using an optical spectrum, Smith et al. (2012) classified the very red donor of the symbiotic fast X-ray transient XTE J1743–363 as a possible >M7 AGB star; however, the donor photometric variability remains unconstrained. CXOGBS J173620.2–293338 and CGCS 5926 were also proposed as candidate SyXRBs spatially coincident with carbon stars (Masetti et al. 2011; Hynes et al. 2014), but their low X-ray luminosity does not exclude white dwarf (WD) accretors.

Sct X-1 thus represents the first confirmed Mira donor star in an X-ray binary, akin to the relatively rare class of D-type symbiotic stars hosting WDs (Allen & Glass 1974). Our results are consistent with the classification scheme of Akras et al. (2019a, 2019b), who classified Sct X-1 as a likely D-type symbiotic binary based on its IR colors. However, the color-based classification is not completely reliable because they did not account for interstellar extinction, which is a substantial correction in the case of Sct X-1. 4U 1954+31 remains the only confirmed Galactic RSG SyXRB (Hinkle et al. 2020), noting that the donor of CXO 174528.79SyXRB290942.8 remains to be spectroscopically confirmed; Gottlieb et al. (2020) could not exclude the possibility of an AGB donor based on the NIR colors.

Our identification of a ≈ 621 day pulsation period in 2MASSJ1835 makes the donor one of the longest-period symbiotic Miras known in the Galaxy (Gromadzki et al. 2009). Long-period Miras (>500 days) are known to be relatively rare; their rarity reflects the brevity of the long-period pulsation phase for lower-mass AGB stars or the rarity of higher-mass AGB stars that spend most of their thermally pulsing phase at longer periods (Vassiliadis & Wood 1993; Marigo et al. 2017; Trabucchi et al. 2019). We can thus constrain the evolutionary stage of the system by comparing the observed pulsation period
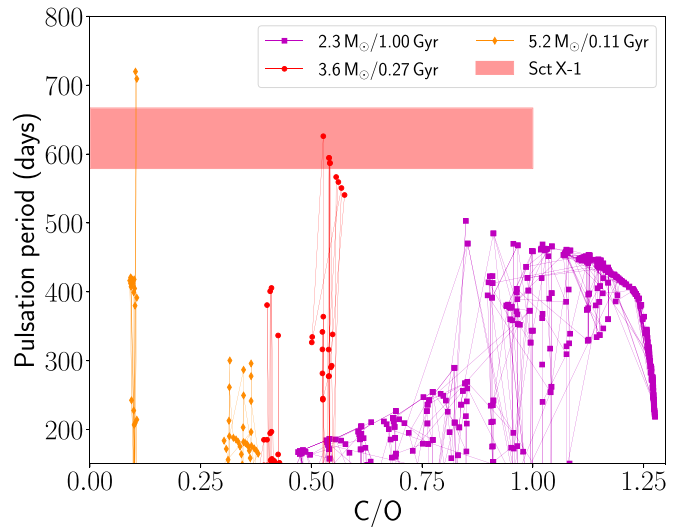
Figure 4. Comparison of the observed pulsation period and surface composition of the infrared counterpart of Sct X-1 (shown in the red shaded region) to evolutionary tracks of AGB stars at different initial masses for solar-metallicity composition ($Z = 0.0152$). We show tracks for three masses as indicated in the legend (along with the corresponding stellar ages), with lines connecting the model epochs in increasing age sequence during the thermally pulsing phase. The period for the dominant pulsation mode at each stage is shown (Trabucchi et al. 2019).

and surface composition (O rich; C/O < 1) to recent AGB evolution and pulsation models (Marigo et al. 2017; Trabucchi et al. 2019, 2021). To this end, we show in Figure 4 the evolutionary tracks[14] of surface composition and pulsation periods for different initial masses.

AGB stars with lower initial masses ($\lesssim 1.5\ M_\odot$) do not evolve to the observed long period (Vassiliadis & Wood 1993; Trabucchi et al. 2019). While the $2.3\ M_\odot$ model does evolve to $P > 500$ days, stars in the initial-mass range ≈ 2.0–$2.5\ M_\odot$ are known to evolve to carbon Miras, inconsistent with the O-rich composition. As shown in Figure 4, we find that stars in the initial-mass range ≈ 3.0–$5.0\ M_\odot$ evolve to the long observed period with an O-rich composition (due to the hot bottom burning process destroying carbon in this higher-mass range; Höfner & Olofsson 2018). We thus favor the scenario where the donor in Sct X-1 had an initial mass of ≈ 3.0–$5.0\ M_\odot$ star, corresponding to a current binary system age of ≈ 0.1–0.3 Gyr. Our conclusions are consistent with the period–age relationship of Mira variables discussed in the recent work of Trabucchi & Mowlavi (2022, their Figures 2 and B.1) and suggest that Sct X-1 is an intermediate-mass X-ray binary.

AGB donors have been long predicted to exist in X-ray binaries based on orbits of radio pulsars (e.g., van den Heuvel 1994); however, known radio pulsars probe binary populations with closer orbits ($\sim$days to months). On the other hand, the formation of wide-orbit SyXRBs requires fine-tuned conditions. If the progenitor binary is too wide, it is likely to get disrupted during the preceding supernova (SN) or never reach the high wind accretion rate required to produce symbiotic activity. If the binary is too close, the NS may merge with its companion during the late-stage evolution of the initially lower-mass secondary star (Iben et al. 1995). The inferred temperature (≈ 2000 K) and luminosity ($\approx 10^4\ L_\odot$) suggest a Mira radius of $\approx 850\ R_\odot$. Taking the current Mira and

---

[14] The tracks were obtained from the online colour magnitude diagram interface at http://stev.oapd.inaf.it/cgi-bin/cmd_3.6.

NS mass to be $\approx 3\,M_\odot$ and $\approx 1.3\,M_\odot$, respectively, the inferred radius constrains the orbital period to be $\gtrsim 12$ yr if the accretion is wind fed (Kaplan et al. 2007), making Sct X-1 possibly the longest orbital period SyXRB known (Hinkle et al. 2019).

Population synthesis calculations (Lü et al. 2012; Yungelson et al. 2019) suggest that AGB donors should be rare among wind-accreting SyXRBs. The NS spin period in Sct X-1 overlaps with the predicted range for AGB donors (Figure 3 in Yungelson et al. 2019), but our estimated orbital period is larger than predicted in their models ($\lesssim 10^3$ days). This discrepancy is a consequence of their models predicting wind-accreting SyXRBs only in the donor's early AGB phase in closer orbit binaries. Specifically, Lü et al. (2012) suggested that AGB donors in the thermally pulsing phase should overflow their Roche lobes, resulting in luminous X-ray emission ($L_X \gtrsim 10^{36}$ erg s^{-1}) unlike known wind-fed SyXRBs. This is also inconsistent with the recent low recent X-ray luminosity of Sct X-1 ($L_X \lesssim 10^{35}$ erg s^{-1}) that is suggestive of wind-fed accretion (Kaplan et al. 2007) from a thermally pulsing AGB star and hence requires a wider orbit than produced in their calculations.

Despite being one of the brightest X-ray sources known from the early days of X-ray astronomy, Sct X-1 demonstrates the potential of wide-field infrared time-domain surveys combined with broadband infrared spectroscopy on moderate-aperture telescopes to understand this population of intrinsically red and obscured sources. We note that donor classifications in SyXRBs have been commonly obtained from optical spectroscopy, while the NIR region contains the most sensitive tracers of the spectral type and luminosity class for late-type evolved stars (Messineo et al. 2021). We thus advocate for a uniform NIR spectroscopic and photometric classification of SyXRBs to constrain their true demographics. In particular, the existence of a significant population of Mira AGBs in SyXRBs would suggest the need for a larger fraction of wide-orbit SyXRB progenitors as well as small birth kicks during the NS formation to keep these systems bound after the SN explosion. In fact, Yungelson et al. (2019) suggested that nearly 80% of SyXRBs may arise from electron-capture SNe due to the resulting low birth kicks. Alternatively, Hinkle et al. (2006) suggested that the evolution scenario in SyXRBs creates ideal conditions for the formation of NSs via the accretion-induced collapse of WDs, making them uniquely suited to search for this predicted population.

Appendix
The Optical Colors of Sct X-1

Using follow-up observations using the MagIC instrument on the Magellan Baade telescope, Kaplan et al. (2007) reported 2MASS J1835 had optical fluxes of $r > 25.2$ mag and $i \approx 23.6$ mag. However, the source was reported in the Gaia catalog at $G \approx 20.4$ mag, $G_{RP} \approx 18.35$ mag, and $G_{BP} \approx 22.34$ mag. Here, we investigate this discrepancy accounting for the different filters used in the observations. Because Sct X-1 is undetected at $\lambda < 1\,\mu m$ and the IRTF library is limited to $\lambda > 0.7\,\mu m$, we use the optical spectrum of the M6-III Mira variable V1334 Sgr from the X-shooter spectral library (Gonneau et al. 2020) to estimate the effects of the heavy reddening on the observed magnitudes. We simulate the extinction to Sct X-1 by reddening the observed spectrum of V1334 Sgr with $E(B - V) = 6.5$ (assuming a Cardelli et al. 1989 extinction law with $R_V = 3.1$), such that the resulting $J - K$ color of the comparison star is the same as 2MASS J1835. Performing photometry on the reddened spectrum using the respective filter profiles,[15] we find expected colors of $G_{RP} - r \approx 8.5$ mag, $G_{RP} - i \approx 2.7$ mag, and $G_{BP} - G_{RP} \approx 10$ mag.

Thus, the large difference between the G_{RP} and r filters for such red sources explains the nondetection of 2MASS J1835 in the r-band observation of Kaplan et al. (2007). However, the relatively blue observed color of $G_{BP} - G_{RP} \approx 4$ mag compared to the simulated M6-III star suggests that pulsational variability is also required to explain the observations. Although the exact dates of observation are not available in Gaia EDR3, the EDR3 observations were obtained over a period of ≈ 34 months, spanning ≈ 1.5 cycles of the estimated pulsation period. For the observed J-band amplitude of ≈ 3.5 mag, the estimated amplitudes in optical filters would be $\gtrsim 6$ mag given the typical wavelength dependence of amplitude in O-rich Miras (Iwanek et al. 2021). Gaia EDR3 reports `phot_bp_n_obs = 2` and `phot_rp_n_obs = 9` for 2MASS J1835, suggesting that the source was indeed detected in more epochs in the redder filter where the source is brighter and has smaller flux amplitudes. On the other hand, the G_{BP} flux is likely dominated by observation epochs near the pulsation maximum where Miras are bluest in color (Reid & Goldston 2002). Thus, the reported Gaia EDR3 colors are expected to be closer to the bluest color of the source near maximum light.

ORCID iDs

Kishalay De ● https://orcid.org/0000-0002-0786-7307
Deepto Chakrabarty ● https://orcid.org/0000-0001-8804-8946
Roberto Soria ● https://orcid.org/0000-0002-4622-796X

---

[15] http://svo2.cab.inta-csic.es/theory/fps/

Michael C. B. Ashley ⓘ https://orcid.org/0000-0003-1412-2028
Charlie Conroy ⓘ https://orcid.org/0000-0002-1590-8551
Matthew J. Hankins ⓘ https://orcid.org/0000-0001-9315-8437
Mansi M. Kasliwal ⓘ https://orcid.org/0000-0002-5619-4938
Robert Simcoe ⓘ https://orcid.org/0000-0003-3769-9559
Tony Travouillon ⓘ https://orcid.org/0000-0002-7279-3658

References

Akras, S., Guzman-Ramirez, L., Leal-Ferreira, M. L., & Ramos-Larios, G. 2019a, ApJS, 240, 21
Akras, S., Leal-Ferreira, M. L., Guzman-Ramirez, L., & Ramos-Larios, G. 2019b, MNRAS, 483, 5077
Allen, D. A., & Glass, I. S. 1974, MNRAS, 167, 337
Arnaud, K. A. 1996, in ASP Conf. Ser. 101, Astronomical Data Analysis Software and Systems V, ed. G. H. Jacoby & J. Barnes (San Francisco, CA: ASP), 17
Bessell, M. S., Brett, J. M., Scholz, M., & Wood, P. R. 1989, A&A, 213, 209
Blum, R. D., Ramírez, S. V., Sellgren, K., & Olsen, K. 2003, ApJ, 597, 323
Cardelli, J. A., Clayton, G. C., & Mathis, J. S. 1989, ApJ, 345, 245
Cash, W. 1979, ApJ, 228, 939
Chakrabarty, D., & Roche, P. 1997, ApJ, 489, 254
Comerón, F., Torra, J., Chiappini, C., et al. 2004, A&A, 425, 489
Cushing, M. C., Vacca, W. D., & Rayner, J. T. 2004, PASP, 116, 362
Davidsen, A., Malina, R., & Bowyer, S. 1977, ApJ, 211, 866
De, K., Hankins, M. J., Kasliwal, M. M., et al. 2020, PASP, 132, 025001
Feast, M. W. 1996, MNRAS, 278, 11
Feast, M. W., Glass, I. S., Whitelock, P. A., & Catchpole, R. M. 1989, MNRAS, 241, 375
Fruscione, A., McDowell, J. C., Allen, G. E., et al. 2006, Proc. SPIE, 6270, 62701V
Gaia Collaboration, Brown, A. G. A., Vallenari, A., et al. 2021, A&A, 649, A1
Gonneau, A., Lyubenova, M., Lançon, A., et al. 2020, A&A, 634, A133
Gottlieb, A. M., Eikenberry, S. S., Ackley, K., DeWitt, C., & Marco, A. 2020, ApJ, 896, 32
Groenewegen, M. A. T., Wood, P. R., Sloan, G. C., et al. 2007, MNRAS, 376, 313
Gromadzki, M., Mikołajewska, J., Whitelock, P., & Marang, F. 2009, AcA, 59, 169
Haniff, C. A., Scholz, M., & Tuthill, P. G. 1995, MNRAS, 276, 640
He, S., Yuan, W., Huang, J. Z., Long, J., & Macri, L. M. 2016, AJ, 152, 164
Hill, R., Burginyon, G., Grader, R., et al. 1974, ApJL, 189, L69
Hinkle, K. H., Fekel, F. C., Joyce, R. R., et al. 2006, ApJ, 641, 479
Hinkle, K. H., Fekel, F. C., Joyce, R. R., et al. 2019, ApJ, 872, 43
Hinkle, K. H., Lebzelter, T., Fekel, F. C., et al. 2020, ApJ, 904, 143

Höfner, S., & Olofsson, H. 2018, A&ARv, 26, 1
Hynes, R. I., Torres, M. A. P., Heinke, C. O., et al. 2014, ApJ, 780, 11
Iben, I. J., Tutukov, A. V., & Yungelson, L. R. 1995, ApJS, 100, 233
Iwanek, P., Kozłowski, S., Gromadzki, M., et al. 2021, ApJS, 257, 23
Joyce, R. R., Hinkle, K. H., Wallace, L., Dulick, M., & Lambert, D. L. 1998, AJ, 116, 2520
Kaplan, D. L., Levine, A. M., Chakrabarty, D., et al. 2007, ApJ, 661, 437
Kholopov, P. N., Samus, N. N., Kazarovets, E. V., & Perova, N. B. 1985, IBVS, 2681, 1
Kirsch, M. G. F., Altieri, B., Chen, B., et al. 2004, Proc. SPIE, 5488, 103
Kleinmann, S. G., & Hall, D. N. B. 1986, ApJS, 62, 501
Koyama, K., Kunieda, H., Takeuchi, Y., & Tawara, Y. 1991, ApJL, 370, L77
Lancon, A., & Rocca-Volmerange, B. 1992, A&AS, 96, 593
Lançon, A., & Wood, P. R. 2000, A&AS, 146, 217
Lü, G. L., Zhu, C. H., Postnov, K. A., et al. 2012, MNRAS, 424, 2265
Marigo, P., Girardi, L., Bressan, A., et al. 2017, ApJ, 835, 77
Martínez-Núñez, S., Kretschmar, P., Bozzo, E., et al. 2017, SSRv, 212, 59
Masetti, N., Munari, U., Henden, A. A., et al. 2011, A&A, 534, A89
Masetti, N., Orlandini, M., Palazzi, E., Amati, L., & Frontera, F. 2006, A&A, 453, 295
Messineo, M., Figer, D. F., Kudritzki, R.-P., et al. 2021, AJ, 162, 187
Mondal, S., Belczyński, K., Wiktorowicz, G., Lasota, J.-P., & King, A. R. 2020, MNRAS, 491, 2747
Moore, A. M., & Kasliwal, M. M. 2019, NatAs, 3, 109
Ramirez, S. V., Depoy, D. L., Frogel, J. A., Sellgren, K., & Blum, R. D. 1997, AJ, 113, 1411
Rayner, J. T., Cushing, M. C., & Vacca, W. D. 2009, ApJS, 185, 289
Rayner, J. T., Toomey, D. W., Onaka, P. M., et al. 2003, PASP, 115, 362
Reid, M. J., & Goldston, J. E. 2002, ApJ, 568, 931
Smith, D. M., Markwardt, C. B., Swank, J. H., & Negueruela, I. 2012, MNRAS, 422, 2661
Trabucchi, M., & Mowlavi, N. 2022, A&A, 658, L1
Trabucchi, M., Wood, P. R., Montalbán, J., et al. 2019, MNRAS, 482, 929
Trabucchi, M., Wood, P. R., Mowlavi, N., et al. 2021, MNRAS, 500, 1575
Udalski, A., Szymanski, M. K., Soszynski, I., & Poleski, R. 2008, AcA, 58, 69
Vacca, W. D., Cushing, M. C., & Rayner, J. T. 2003, PASP, 115, 389
van den Heuvel, E. P. J. 1994, A&A, 291, L39
Vassiliadis, E., & Wood, P. R. 1993, ApJ, 413, 641
Whitelock, P., Marang, F., & Feast, M. 2000, MNRAS, 319, 728
Whitelock, P. A. 1987, PASP, 99, 573
Whitelock, P. A., Feast, M. W., & Van Leeuwen, F. 2008, MNRAS, 386, 313
Wilms, J., Allen, A., & McCray, R. 2000, ApJ, 542, 914
Wood, P. R. 2000, PASA, 17, 18
Wood, P. R., & Sebo, K. M. 1996, MNRAS, 282, 958
Wright, E. L., Eisenhardt, P. R. M., Mainzer, A. K., et al. 2010, AJ, 140, 1868
Yungelson, L. R., Kuranov, A. G., & Postnov, K. A. 2019, MNRAS, 485, 851